2020 AIAA SciTech Forum, 6-10 January 2020, Orlando, Florida, USA
DOI:10.2514/6.2020-1286

Progress towards a Rapid Method for Conceptual Aerodynamic Design for Transonic Cruise

Simon A. Prince[1], Davide di Pasquale[2]
and Kevin Garry[3]

School of Aerospace, Transport & Manufacturing, Cranfield University, Cranfield, Bedfordshire, UK.

Results are presented from a study aimed at demonstrating the accuracy and efficiency of a lower order aerodynamic prediction method for transonic cruise flows around aircraft configurations, including conventional swept wing-body and also blended wing-body designs. The Viscous Full Potential (VFP) method, coupling the solution of the full potential equations with the integral boundary layer equations can yield data of almost equivalent accuracy as Navier-Stokes based CFD methods but at 0.5% - 2% of the physical time. In addition it is shown, using both the VFP approach and Delayed Detached Eddy Simulation (DDES) that the flow physics of the stall mechanism associated with blended wing-body configurations is far more complex than that experienced on more conventional swept-tapered wings. The mechanism appears to involve an initial tip stall but also involves highly 3D vortical flows inboard on the upper surface of the wing which significantly distorts the transonic shock wave.

I. Nomenclature

a	=	speed of sound (m/s)
α	=	angle of attack (deg)
C_p	=	pressure coefficient
C_D	=	drag force coefficient.
C_f	=	surface skin friction coefficient
C_L	=	lift force coefficient.
c	=	chord length (m)
e	=	denotes top edge of the boundary layer
δ	=	boundary layer thickness (m)
δ^*	=	boundary layer displacement thickness (m)
Φ	=	velocity perturbation potential function
H	=	boundary layer shape factor
M	=	Mach number
θ	=	boundary layer momentum thickness (m)
Re_c	=	Reynolds number based on chord (root chord for a BWB, otherwise mean aerodynamic chord)
ρ	=	density (kg/m^3)
t	=	time (s)
U	=	freestream velocity (m/s)
u, v, w	=	velocity components in the x, y and z directions respectively (m/s)
x, y, z	=	cartesian co-ordinates, where the x-direction corresponds to streamwise flow direction at zero α.
ξ	=	co-ordinate normal to, and out from, the wall surface (m)

[1] Senior Lecturer, School of Aerospace, Transport & Manufacturing, Cranfield University. AIAA Senior Member.
[2] Research Fellow, School of Aerospace, Transport & Manufacturing, Cranfield University.
[3] Professor, School of Aerospace, Transport & Manufacturing, Cranfield University. AIAA Fellow.

II. Introduction

The accurate and timely conceptual design of a high speed aircraft requires robust analysis methods that provide data rapidly but at the appropriate fidelity. The conceptual phase of design is the least costly stage of the whole design process, but is the stage where downstream cost associated with bad design is often embedded. The ability to undertake trade off studies, assess the benefits of integrating new technologies at a whole aircraft and Multiphysics level, and to do this rapidly and with an acceptable physical accuracy is of prime importance. There has been a recent tendency in some companies, however, to implement very high order physical methods too early in the design process with the result of constraining the breadth and scope of the possible trade-off synthesis where the available computing resources might be better employed using methods of lower but still appropriate level of physical fidelity and accuracy, to advance the design more quickly and effectively.

This paper presents some of the aerodynamic assessments using a lower order aerodynamic simulation tool being developed for a conceptual design environment for low speed and transonic cruise aircraft configurations under a collaborative UK research project called APROCONE (Advanced Product Concept Analysis Environment) and follows an earlier paper focusing more on the validation of these methods [1]. While the project aimed to couple aerodynamic configuration, propulsion and aeroelastic simulation methods together in a holistic whole aircraft system design method for conceptual design, this paper focuses on the rapid aerodynamic prediction aspects of the project. First data from a validation exercise on a transonic wing body are presented to demonstrate the accuracy and efficiency of the lower order approach, before the results of a detailed aerodynamic assessment of the transonic performance of a conceptual civil blended wing body (BWB) airliner are presented. While much work has been published on the aerodynamics of blended wing configurations at low speed, very little information is available on the transonic performance of such configurations, particularly with regards the complex three-dimensional stall that is known to occur. This was the focus of a study within the APROCONE project, results from which are presented in this paper.

III. The Transonic Flow Methodology

A. Governing Equations

The aim of the APROCONE project was to develop and demonstrate a multiphysics design environment that would provide conceptual design data in a rapid, timely and secure manner across corporate boundaries. With this in mind a study was undertaken to identify the correct fidelity of physical airflow modelling that would provide the required physical data to the appropriate accuracy and with the highest speed. For transonic cruise design the requirements are for a method that would provide surface pressure, surface friction and boundary layer state data (thickness, displacement thickness, momentum thickness and form factor) where the boundary layers are attached. While it is important to be able to assess the stall characteristics of a configuration, the conceptual design requirements for a transonic cruise aircraft is for maximum lift to drag capability at a design point with appropriately safe margins before boundary layer separation and consequent buffet onset (both in terms of Mach number and angle of attack). Similarly, an efficient transonic cruise aircraft design would not operate in a condition where shock waves become strong enough to induce boundary layer separation. A suitable cruise design method for aerodynamics was therefore deemed to be an attached boundary layer method, with the ability to capture the relatively weak shock waves encountered in such a flight regime.

The most appropriate method reviewed in the study was found to be a coupled full-potential solver with a boundary layer equation solver allowing the attached 3D skewed boundary layers, typically encountered in flight, to be resolved. The potential flow equations are obtained from reducing the Navier-Stokes equations by neglecting viscosity and assuming the flow to be isentropic and irrotational. This reduced form of the governing equations allows the continuity equation to be derived in terms of the velocity potential function Φ. The isentropic assumption limits the validity of the method to cases where no shock waves exist in the flow field, or where the shock waves are so weak that the errors in the calculation of pressure and velocity are minimal, but this situation is entirely consistent with the desired flow characteristics for transonic cruise.

The full velocity potential equation, for an irrotational, inviscid, isentropic flow, in terms of Cartesian coordinates (*x,y,z*) is given as:

$$\left(1-\frac{\bar{\Phi}_x^2}{a^2}\right)\bar{\Phi}_{xx}+\left(1-\frac{\bar{\Phi}_y^2}{a^2}\right)\bar{\Phi}_{yy}+\left(1-\frac{\bar{\Phi}_z^2}{a^2}\right)\bar{\Phi}_{zz}-2\frac{\bar{\Phi}_x\bar{\Phi}_y}{a^2}\bar{\Phi}_{xy}-2\frac{\bar{\Phi}_x\bar{\Phi}_z}{a^2}\bar{\Phi}_{xz}-2\frac{\bar{\Phi}_y\bar{\Phi}_z}{a^2}\bar{\Phi}_{yz}$$
$$-2\bar{\Phi}_x\bar{\Phi}_{xt}-2\bar{\Phi}_y\bar{\Phi}_{yt}-2\bar{\Phi}_z\bar{\Phi}_{zt}-\bar{\Phi}_{tt}=0 \tag{1}$$

where the velocity potential Φ is defined by:

$$V=\sqrt{u^2+v^2+w^2} \;=\; \nabla\bar{\Phi} \tag{2}$$

such that:

$$u=\bar{\Phi}_x=\frac{\partial\bar{\Phi}}{\partial x}, \qquad v=\bar{\Phi}_y=\frac{\partial\bar{\Phi}}{\partial y}, \qquad w=\bar{\Phi}_z=\frac{\partial\bar{\Phi}}{\partial z} \tag{3}$$

and the time, *t*, is in the unsteady terms. If the flow is steady, the last four terms of the equation are neglected.

The boundary layer equations can be simplified by using averaged quantities obtained by integrating through the boundary layer, yielding the integral boundary layer equations. The three-dimensional integral boundary layer equations and their solution for straight, swept and tapered wing flows, and their solution are given by Smith [2]. For simplicity the 2D integral boundary layer equations are given here for illustrative purposes. The boundary layer momentum equation is given as:

$$\frac{d\theta}{dx}=\frac{C_f}{2}-\frac{\theta}{U_e}\frac{dU_e}{dx}(H-2-M_e^2) \tag{4}$$

and is solved together with an auxiliary equation, called the entrainment equation, which describes the inflow of external air into the boundary layer as it thickens in the streamwise direction, typically given as:

$$\frac{d(\delta-\delta^*)}{dx}=C_E-\frac{\delta-\delta^*}{U_e}\frac{dU_e}{dx}(1-M_e^2) \tag{5}$$

where C_E is the entrainment coefficient, which is a function of the boundary layer shape factor, $H = \delta^* / \theta$. The terms U_e and M_e are the streamwise velocity component and corresponding Mach number at the top edge of the boundary layer, and the boundary layer displacement thickness, δ^*, and momentum thickness, θ, are defined as:

$$\theta=\int_0^{\delta}\frac{\rho U}{\rho_e U_e}\left(1-\frac{U}{U_e}\right)d\xi \tag{6}$$

$$\delta^*=\int_0^{\delta}\left(1-\frac{\rho U}{\rho_e U_e}\right)d\xi \tag{7}$$

B. The VFP Solver

The baseline VFP solver employed in this study was that developed by the UK Royal Aerospace Establishment (RAE) and Aircraft Research Association (ARA) for the UK aircraft industry during the 1980's, and is now available commercially from IHS ESDU [3,4]. The code was further developed and optimized during the course of the APROCONE project to including better modelling of wing-body configurations rather than the just the wing alone. The wing geometry is input as a series of section profiles defined from the root to the tip, along with the corresponding

location, relative to the fuselage reference point, of the local leading edge, the chord length and the local twist angle setting. The geometry input file allows for the rapid alteration of such geometric features as leading edge sweep, taper, local dihedral, crank location and twist setting, involving the modification of just a few parameters which can be done manually or as part of a computational optimization algorithm.

The VFP program solves the flow around the isolated fuselage body separately, and then uses this flowfield to calculate the inflow for the wing calculation. This approach provides a quick and reasonably accurate method of capturing the interference effects of the body on the wing flow. This is much more important in the prediction of the overall aerodynamic characteristics of a wing-body configuration than the interference effects of the wing on the body, which is currently neglected for the purposed of this study, though modelling of this effect will be introduced in future work. The fuselage flowfield is calculated using the classical method of Von Karman [5], which solves the Stokes-streamline problem for an arbitrary body geometry, defined in a separate input file. The method calculates the zero incidence surface pressure on the isolated fuselage, and off-surface velocity and pressure field around it. The effect of angle of attack on both the surface pressure and the flow field is calculated using the slender body theory based method of de Jarnette [6]. The increment in the inflow Mach number along the span of the wing is then calculated and applied to the VFP solution of the wing flow, thereby resolving the influence of the fuselage on wing.

The contribution of fuselage to the aerodynamic forces and moments of the configuration are calculated by the surface integration of the predicted fuselage surface pressure distribution. The viscous friction contribution from the fuselage is estimated by assuming a flat plate Blasius skin friction distribution on an equivalent wetter surface area. It is also assumed that the angles of attack of interest to transonic cruise are limited to low values, at which there will not be any large scale boundary layer separations leading to vortex formation and non-linear vortex lift.

The VFP code automatically generates the separate computational grids around both the fuselage and the wing, details for which are provided in reference [3]. For this study the wings investigated are modelled with meshes of 135,432 cells, wrapping an O-topology grid around the wing with 162 cells wrapped around the wing, 38 cells along the span and 22 cells outwards from the wing surface. The fuselage models were meshed with 33 cells along the axis, 32 cells around its circular half perimeter (assuming symmetric geometry and flow about the $y = 0$ (wing centreline) plane, and 32 cells outwards from the fuselage surface. The wake characteristics are calculated to allow for wake relaxation and the correct wing spanwise circulation to be resolved.

The code uses a relaxation algorithm to solve the finite difference form of the full three-dimensional velocity-potential equations which are coupled with the semi-inverse, swept / tapered integral boundary layer method of Ashill and Smith [2, 7]. The boundary layer displacement thickness obtained from the boundary layer solver was then used to update the surface shape by the addition of the resulting displacement thickness distribution before another FP calculation was performed on the updated surface geometry. The convergence criteria was set as a maximum absolute change in value of velocity perturbation potential anywhere in the flow, reduced to an order of 10^{-6}.

C. The Navier-Stokes Solver

For the detailed analysis of the onset boundary layer separations and the subsequent stalled flow fields it is necessary to employ a high resolution Navier-Stokes (N-S) flow solver. For the attached flow cases at and near the cruise condition, N-S data was computed in order to validate the VFP data. In the case of the Cranfield BWB performance assessment, where no transonic experimental data exists, the two methods were used to validate each other up to incipient stall, beyond which no VFP solutions could be obtained as the method is then invalid for the flow state being simulated. A modern commercial, compressible flow, Navier-Stokes solver was employed to obtain high resolution simulations of the flows of interest. This finite-volume solver employed the Roe approximate Riemann solver for shock capturing, with a second order scheme in both space and time to obtain converged steady flow solutions as starting solutions for unsteady Delayed Detached Eddy Simulation (DDES). Hybrid unstructured meshes were employed with prismatic embedded cells grown out from the wall surfaces, whereby the boundary layers were captured within 25 – 30 cell layers, and with the first cell height set at 1×10^{-5} times the tip chord in order to ensure values of y^+ of the order of 1.0. While a number of turbulence models were employed within the DES framework for the RBC12 test case, only the k-ω SST model based DES results are presented in this paper.

A time step of 1 millisecond was used with a maximum of 50 iterations per time-step. Grid insensitivity was demonstrated in all cases, the convergence criteria being overall force coefficient convergence together with residual convergence to at least 10^{-4}.

IV. Test Case Details

A. The ARA RBC12 Wing Body Validation Case

For the purposes of validation of the VFP method the Aircraft Research Association RBC12 wing-body test case is used. Reference 1 also presents validation results for the RAE Wing 4 wing-body test case. The RBC12 configuration is a generic wing-body configuration, based on a 1990s standard transonic civil airliner configuration that was developed as a research model to test measurement techniques in their transonic wind tunnel. Fig 1 presents the basic dimensions of the model along with a photograph of the model mounted in the ARA Transonic Wind Tunnel in Bedford, UK [8]. The RBC12 half model has a swept and tapered cranked wing with a quarter chord sweep of 25°, with a semi-span of 1.085m and a mean aerodynamic chord of 0.279m, giving an aspect ratio of 7.78.

The model has been tested in the Transonic Wind Tunnel, located on the floor mounted 5-compunent strain gauge balance measuring the force and moments on the combined wing and fuselage together. The Dynamic Pressure Sensitive Paint technique was used to acquire surface pressure distributions on the wing upper surface. Tests were conducted in the Mach number range 0.7 – 0.84, (Re_c between 2.8 million and 3.9 million) with results published in reference [8]. The validation case presented here is for the Mach 0.8 condition where Re_c = 3.75 million.

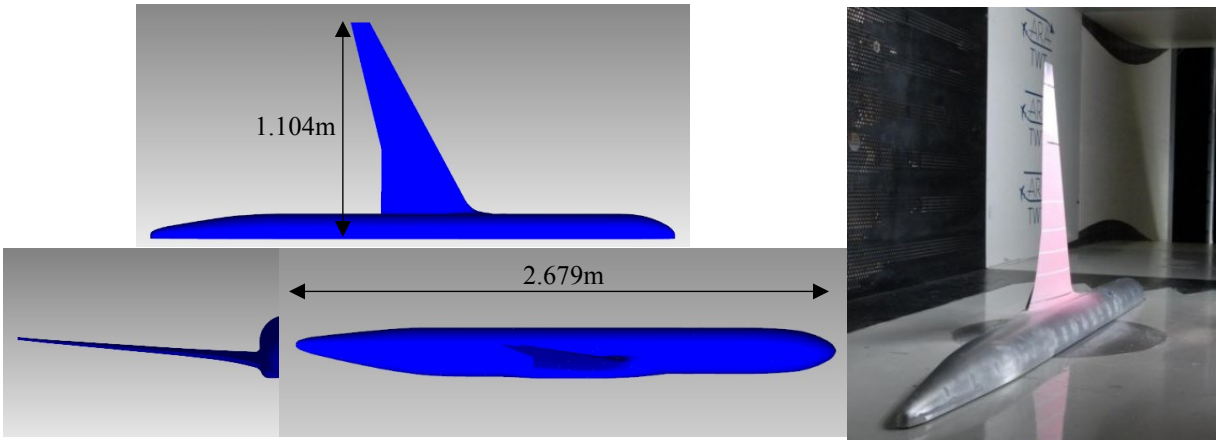

Fig. 1. The ARA RBC12 geometry and the model in the ARA Transonic Wind Tunnel [8].

B. The Cranfield BWB-11 Blended Wing Body Case

The VFP code and the Navier-Stokes solver were employed together in the analysis of the Cranfield BWB-11 blended wing body in order to provide more insight into the transonic performance of this class of configuration, particularly in stall for which condition there is very little information in the literature. The BWB-11 configuration was developed at Cranfield University as a research geometry for the assessment of blended wing body aircraft and was derived from the Cranfield Aerospace / BAe Systems Kestrel BWB demonstrator [10] and the Boeing X-48B demonstrator [11], both of which flew well below transonic condition. The BWB-11 geometry was developed for a conceptual Airbus A380 class large civil airliner, designated Eagle-Ray, the particular variant of the configuration assessed here being that without the tip winglets, shown in fig 2.

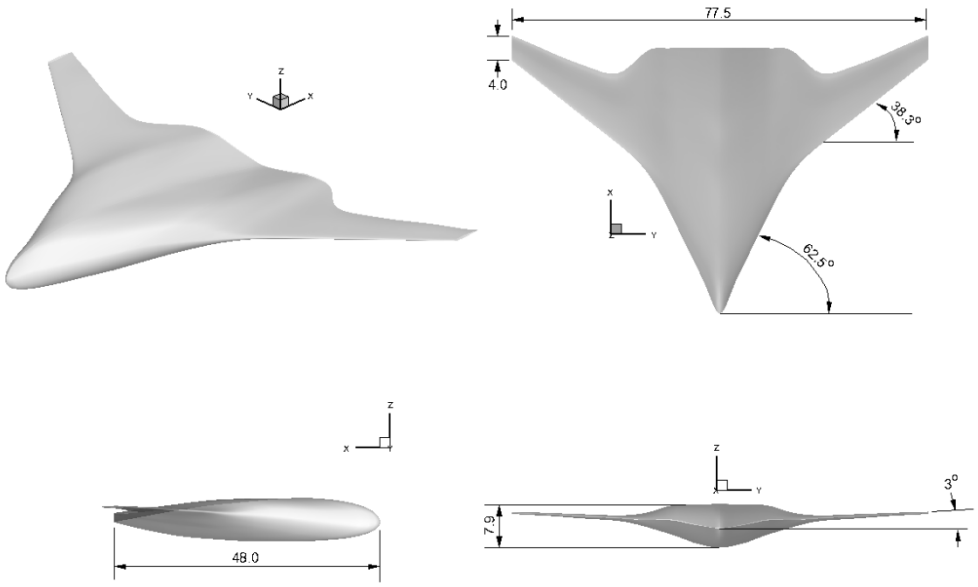

Fig. 2. The full scale Cranfield BWB-11 configuration without winglets (units in metres).

V. Results

This section presents a sample of validation test data, whereby the VFP and DDES solver results are compared with experimental data for the RBC12 configuration, as well as more detailed analysis of the aerodynamic characteristics of the Cranfield BWB-11 blended wing body, again using both the VFP and DDES solvers. For the BWB, with the absence of experimental data for transonic cruise conditions, both VFP and unsteady Navier-Stokes are compared for the low angle of attack, pre-stall, conditions, while only the Navier-Stokes results are presented for the analysis of the complicated post stall flows.

A. Validation Example: Fuselage Flow Prediction

Figure 3 presents an example of the accuracy of the fuselage potential flow model for a representative aircraft forebody of elliptical nose shape. This example is for a Mach 0.11 flow around the body at zero angle of attack, where the experimental Reynolds number, based on body diameter, was 0.65×10^5.

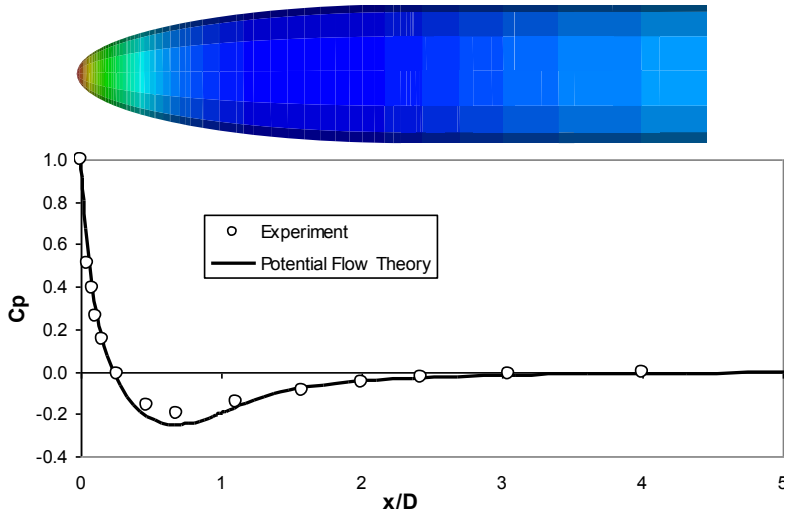

Fig. 3. Comparison of VFP predicted and experimentally measured surface pressure on an elliptic nosed fuselage nose.

The agreement between the predicted and measured surface pressure is certainly good enough for a rapid conceptual analysis tool to allow the integrated pressure loads to be calculated for the force and moment contribution to the overall configuration. For the higher Mach numbers of interest, it is assumed that there are no shock waves or boundary layer separations, and the compressibility effects are dealt with using the Prandtl-Glauert compressibility transformation.

B. Validation Example: The ARA RBC12 Transonic Wing-Body Configuration

The grid sensitivity analysis for the DDES study on RBC12 found that mesh insensitivity was achieved with a cell count of approximately 20 million. This was done using progressive mesh adaption to the wing shock wave and wake until force and moment coefficients, to three significant figures, became mesh independent. Since the simulations were required for a separate study of flow unsteadiness levels pre and post buffet onset, the DDES solver was used to acquire 0.5 seconds of simulated flow. The initial steady Navier-Stokes calculations (k-ω SST turbulence model) took around 9 hours for each flow condition to converge on 128 core processors of a modern parallel cluster machine, while the acquisition of 0.5 seconds of DDES simulation data typically took about 5 days run time on the same processors.

The VFP calculations were started by the calculation of the flow for the lowest angle of attack, which in this case was -0.5°. This calculation took typically 7 minutes on single processor of a modest desktop PC. This flow solution was then used as the starting solution for the next higher angle of attack calculation, and this process was continued until the highest angle of attack before the process broke down due to the failure of the boundary layer solver with the onset of significant separation. Pitch polars were obtained using VFP with angle of attack increments of 0.5°. With each subsequent angle of attack simulation taking approximately 2 minutes, an entire polar up to stall onset could be completed in less than an hour.

Figure 4 presents a comparison of the surface meshes for the VFP analysis and the coarsest, pre-adaption, mesh used in the N-S / DDES study, along with the comparison of the computed surface pressures predicted by each method for the Mach 0.8, α = 2.4° case. It can clearly be seen that the VFP circular sectioned fuselage geometry is an approximation of the non-circular section RBC12 fuselage, but since the VFP code is designed to be a rapid conceptual design tool rather than a detailed analysis tool, such approximations are deemed to be acceptable as long as the resulting force and moment and wing flow conditions are accurate enough for the purpose.

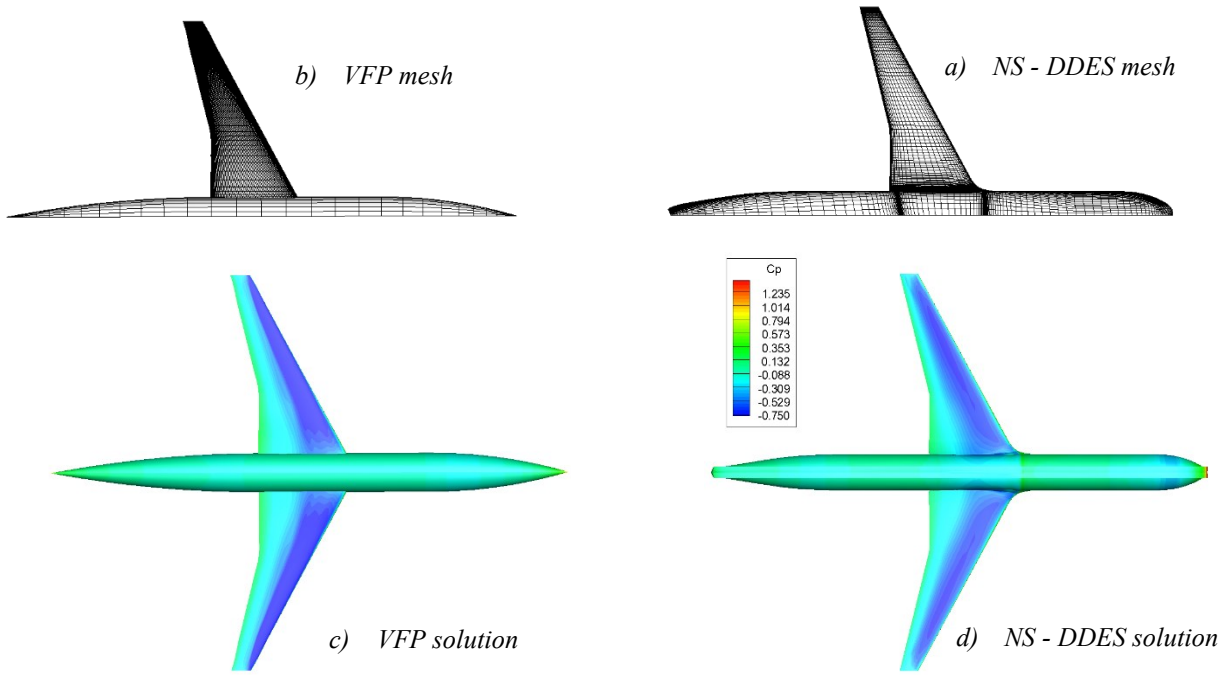

Fig. 4. Comparison of VFP and Navier-Stokes (DDES) predicted surface Cp contours for the RBC12 configuration, M=0.80, $Re_c = 3.75x10^6$, $\alpha = 2.4°$.

Scrutiny of the predicted wing surface pressures reveals that the VFP code successfully predicts the upper surface swept shock wave acceptably well for a lower order method, yielding a result in between 1.3 to 0.4% of the time required for the fidelity solution. Figure 5 presents the comparison of the measured lift and drag characteristics in the wind tunnel with those predicted by the VFP and the Navier-Stokes (only four conditions being computed in the time available) simulations. Data for the forces on the wing have been extracted for comparison from the computed data. As expected, the N-S / DDES simulation did a very good job in accurately calculating the time averaged lift and drag characteristics for both the complete configuration and also the contribution from the wing, far better than the purely steady N-S simulation whose results were presented in reference 1. These simulations also allow for the analysis of unsteady flow effects, such as shock wave oscillations prior to boundary layer separation (buffet onset), which the VFP approach cannot provide but is not needed in conceptual aircraft design.

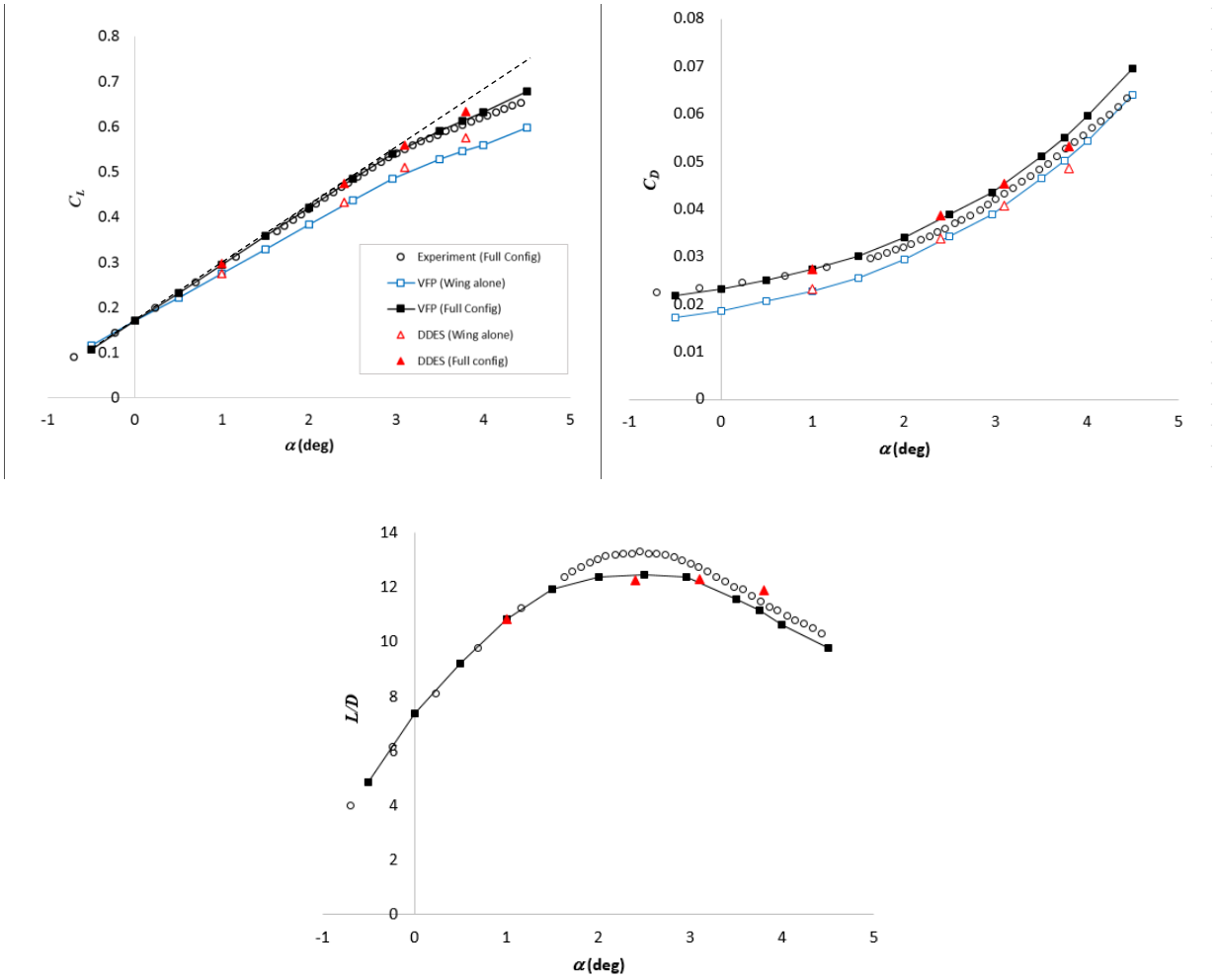

Fig. 5. Comparison of VFP and Navier-Stokes (DDES) predicted force characteristics for the RBC12 configuration, M=0.80, $Re_c = 3.75x10^6$.

The VFP resolved forces are seen to be remarkably good, where their agreement with the experimental measurements are at least as good as those obtained from the N-S / DDES simulation but achieved in two orders of magnitude less time. Surprisingly, the VFP result successfully resolves the non-linearity in the lift trend due to the onset of shock induced viscous effects. The coupled boundary layer method within the VFP solver can predict laminar separation bubbles and small trailing edge separated flow as regions where the local skin friction coefficient drops to zero. The agreement between the VFP predicted drag and the experimental data is very good at low angle of attack,

as is the N-S DDES derived drag. The VFP solver, however, marginally overpredicts drag force at the higher angles of attack, but is still within the bounds of acceptability. In fact the VFP resolved drag characteristics are only marginally less accurate than those obtained using the Navier-Stokes solver at considerably higher cost in time. This is also reflected in the comparison for lift to drag ratio, where up to α=1.5^o both prediction methods provide almost exact figures compared with the measured data. At higher angles of attack both prediction methods are seen to underpredict the lift to drag ratio by up to 8%. Importantly the VFP solver is seen to correctly identify the angle of attack for peak *L/D* which would be the cruise condition for this Mach number / Reynolds number case, and is an important factor in conceptual aircraft design.

Detailed analysis of the wing flows where the resolution of the upper surface shock strength and location are important, shows that the VFP method can successfully capture these upper surface shock characteristics very well, to a standard more than acceptable for conceptual design analysis. Figure 6 presents the comparison of the experimentally measured (dynamic pressure sensitive paint) upper surface pressure contours with the corresponding predicted results for the Mach 0.8, α = 3.76^o case. While the N-S / DDES solution seems to resolve the inboard shock bifurcation very well with a sharply captured forward shock feature, the VFP result still successfully captures the effect, and resolves the shock wave to a sharp enough standard to allow optimization, for instance to minimize wave drag at this condition. The VFP solution has also successfully resolved the shock unsweep at the tip which is seen in the experimental measurements.

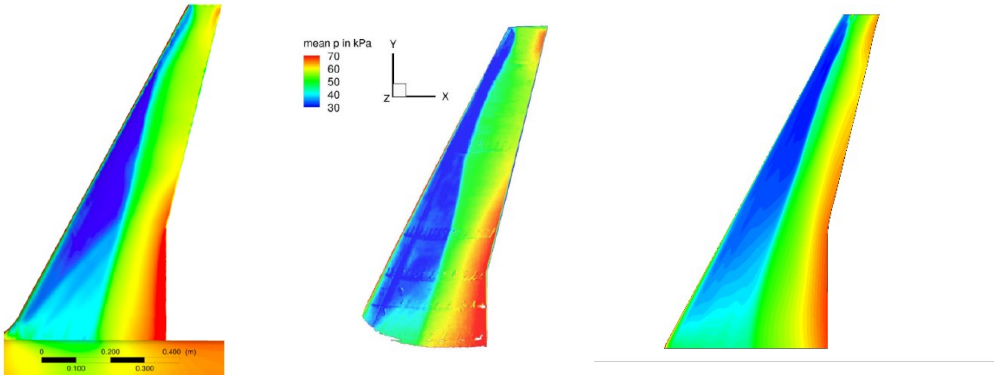

a) NS - DDES *b) Experiment [8]* *c) VFP*

Fig. 6. Comparison of measured (Dynamic PSP) and computed surface pressure contours for RBC12, M=0.80, $Re_c = 3.75x10^6$, $\alpha = 3.76^o$.

In summary the RBC12 validation exercise, along with others undertaken in the APROCONE project, effectively demonstrated the remarkable accuracy and efficiency of the coupled Full-Potential / Boundary Layer solver approach for the conceptual design analysis of transonic cruise aircraft configuration.

C. Aerodynamic Assessment of the Cranfield BWB11 Eagle Ray Blended Wing Body Aircraft Concept

Having successfully validated the VFP and the Navier-Stokes DDES solver on several challenging transonic wing-body test cases, the authors were confident enough to apply the methods to assess the aerodynamic performance of the BWB-11 blended wing body configuration in the transonic regime, to help understand the complex compressible airflows in the absence of experimental data.

Figure 7 presents a comparison of the computations grids used by each of the solvers. Both meshes were developed using the same strategies as was used for the RBC12 study, including the calculation of the first cell height using the flow Reynolds number, which for this case, for the full aircraft configuration, was Re_c=7.4x10^8. The structured VFP mesh, where in this case no fuselage definition is required, comprised 135,432 cells, while the Navier-Stokes mesh was a hybrid unstructured mesh with prismatic boundary layer embedded cells which, following a grid sensitivity exercise, comprised 14 million cells. The difference in cell densities used in the two approaches is clearly evident in fig 7.

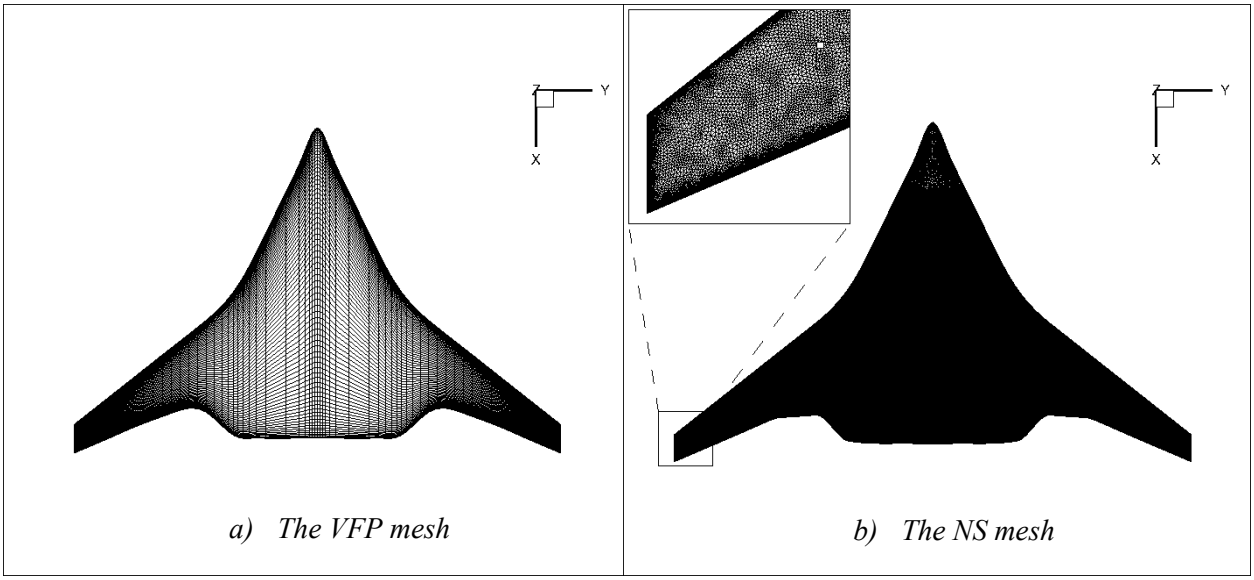

a) The VFP mesh *b) The NS mesh*

Fig. 7. The computational meshes for the Cranfield BWB-11 study.

Pitch sweeps were conducted at Mach numbers of 0.70, 0.75, 0.80 and 0.85 with the Reynolds number fixed at that calculated for the Mach 0.80 cruise condition, being Re_c=7.4x10^8. Again the VFP solver computed complete pitch sweeps at all four conditions, starting from α=0^o in this case, and proceeding until the solver diverged due to incipient separation effects in the boundary layer equation solver. The first starting calculation took around 6 minutes in each case, while the subsequent higher angle of attack calculation took around 2 minutes each, all on a single Xeon 3.6Gz processor. The Navier-Stokes DDES calculations however took around 5 hours to compute the initial steady state solution and a further ~2 days each in DDES mode to obtain 1 seconds worth of data on 8 Xeon 3.6Gz processors in parallel. This comparison in efficiency of the two methods for the analysis of the attached flow cases clearly demonstrates the huge benefit of using lower order methods of appropriate fidelity and accuracy where they are valid, and only using the highest fidelity, highest cost methods where the physics dictates their use (such as for resolution of unsteady effects or in highly separated flows).

Figure 8 presents the comparison of the predicted force characteristics of the BWB-11 configuration at the cruise condition of Mach 0.80. The VFP solver detected flow breakdown, and therefore diverged, at 5^o angle of attack, while the Navier-Stokes solver was used to acquire flow solutions all the way up into deep stall at α = 12^o. Up to about 6^o angle of attack the time averaged DDES result did not depart very much from that obtained from the steady RANS starting solution. Above this, there were some differences, but very little can be concluded from this without the provision of experimental data. What is very striking from the force data in figure 8 is the remarkable agreement between the VFP derived force coefficients and those derived from the higher fidelity method, particularly the drag data, which is usually difficult to predict. This gives confidence that, at least in the attached flow regime, the predicted flow fields are likely to be a good representation of the real physical flow.

The analysis shows that the cruise attitude for this configuration is likely to be close to 2^o angle of attack where *L/D* is at its peak, not dissimilar to a conventional wing-body aircraft design. The peak L/D appears to be around 17 to 18, compared with around 12 for the RBC 12 configuration, which supports the view that blended wing body configurations can be more aerodynamically efficient than conventional wing-bodies. The stall characteristics also look relatively benign, with no sudden loss of lift.

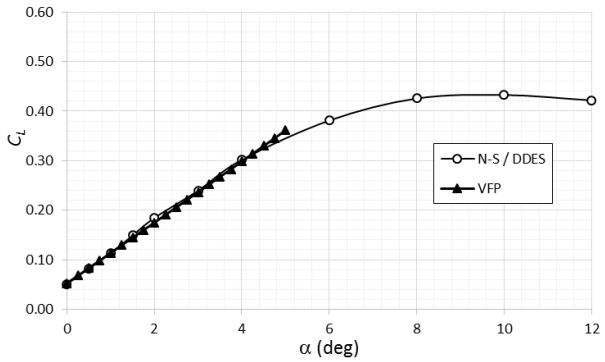

a) Lift coefficient

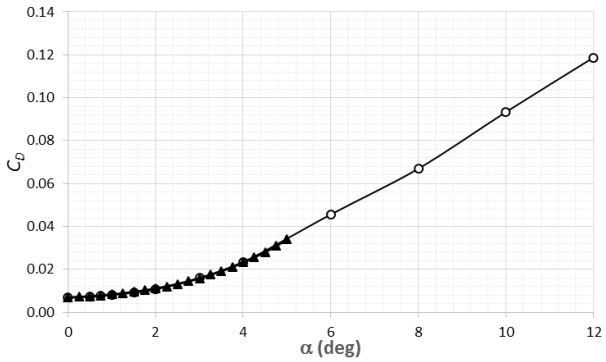

b) Drag coefficient

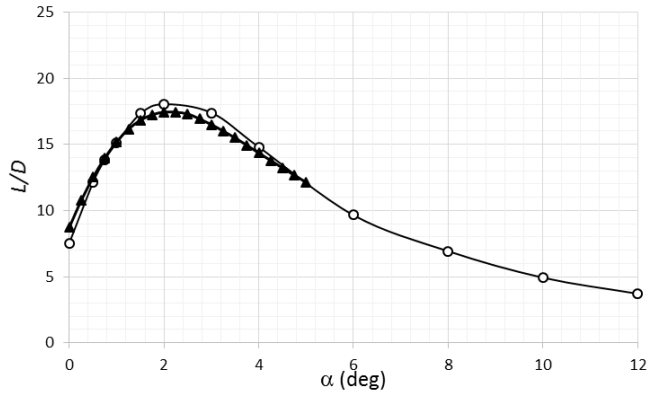

c) Lift to drag ratio

Fig. 8. Comparison of predicted force characteristics, M=0.80, Re_c=7.4x10^8.

Figure 9 compares the VFP resolved upper surface pressure distribution at the three highest Mach number conditions at the optimum α=2^o attitude, with a corresponding instantaneous result using the Navier-Stokes solver. For the Mach 0.75 case the flow looks benign, with no evidence of any shock wave over the upper surface and no separations evident in the surface skin friction lines obtained from the Navier-Stokes solution. The agreement between the two methods is also remarkably good, the only difference being a degradation of the leading edge suction towards the tip which is predicted by the Navier-Stokes solver, but is not in the VFP solution.

At the Mach 0.80 condition the flow over the upper surface is marginally supercritical with the VFP solver predicting a very weak shock wave. The corresponding N-S / DDES solution predicts the flow to be significantly unsteady with the weak incipient shock wave being highly unsteady and sensitive to the unsteadiness in the underlying turbulent boundary layer. The instantaneous upper surface pressure plot in fig 9b) indicates that there may be multiple weak shock waves in motion that, at higher Mach number, coalesce into a single swept shock wave. These weak shock features, however, are not strong enough to significantly deflect the surface skin friction lines, let alone separate the boundary layer. At the highest Mach number investigated, M = 0.85, there is one upper surface shock wave, which both solvers predict to be swept outboard, but which unsweeps inboard to become nearly normal to the flow at the BWB centerline. Interestingly the N-S / DDES prediction indicated only small levels of unsteadiness at the tip where the shock wave in strongest, and where the skin friction lines are seen to be deflected by the shock. The VFP code predicts the shock wave to be about 10% more rearward at the centerline than is predicted in the Navier-Stokes solution. Also the VFP solver predicts higher suction pressures near the tip ahead of the shock. Without a good set of experimental data it is not possible at this stage to conclude which is most representative of the real physical flow. However, the agreement between the two predicted flows are generally remarkably close, and it is possible to say that

the VFP solver would be accurate enough for use as a conceptual design tool to look at configuration performance trade- offs, and for cruise configuration optimization.

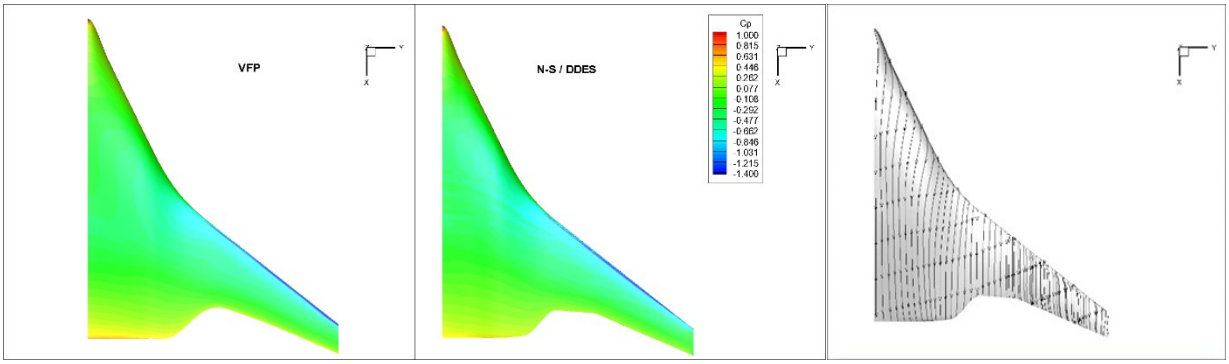

a) M = 0.75

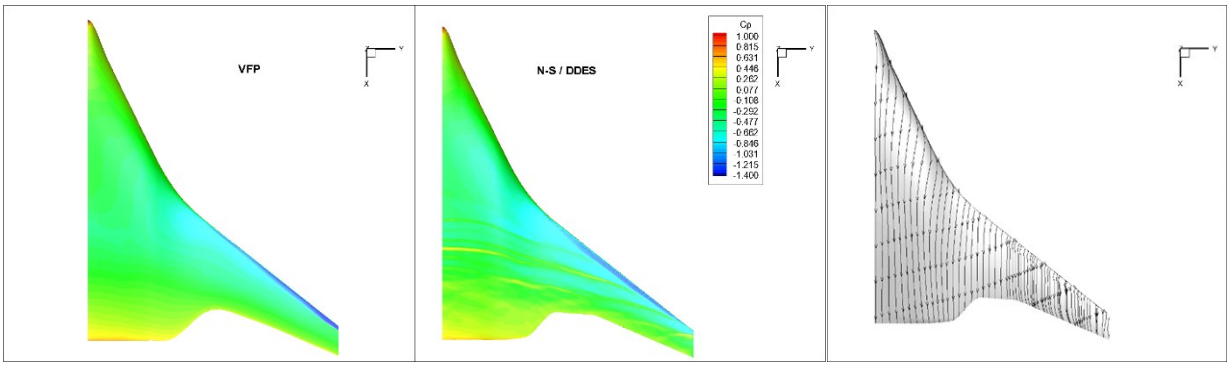

b) M = 0.80

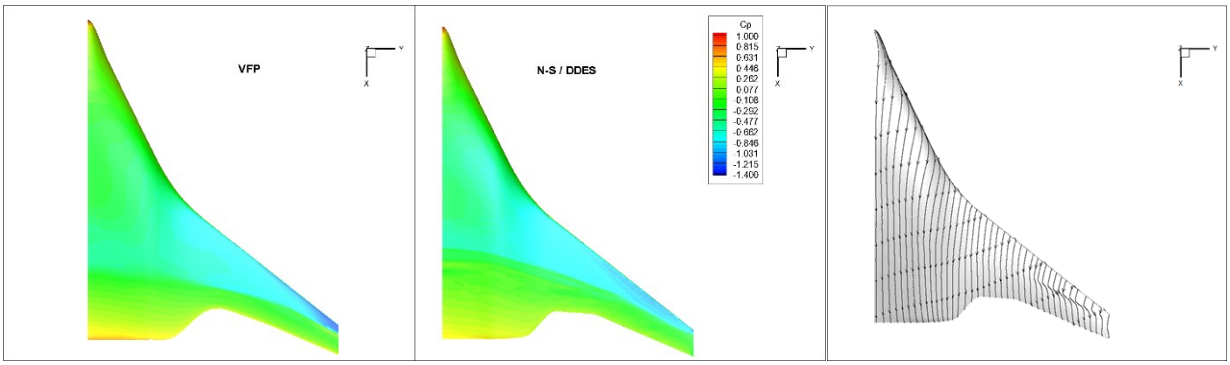

c) M = 0.85

Fig. 9. Comparison of the VFP computed upper surface pressures on the Cranfield BWB-11 with those from the NS-DDES solver, together with the NS-DDES resolved surface skin friction lines. Re_c = 7.4 x10^8, α = 2^o.

For the assessment of the complex flow physics at high angle of attack it is necessary to rely on experiment and on high resolution unsteady computational fluid dynamics simulation based on the Navier-Stokes equations. Figure 10 presents, for the Mach 0.85 case, the time averaged upper and lower surface pressure distributions extracted from the N-S / DDES solutions at the highest angles of attack studied, together with a corresponding image of the computed surface skin friction pattern at an instant in time. At an angle of attack of 6^o, the flow is predicted to have undergone a shock induced separation outboard of the crank, with the tip flow being fully separated. The leading edge crank and

the local thickening of the body towards the centerline acts to reduce the leading edge expansion and prevent the separation progressing inboard, although the shock wave curves in to become normal over the innermost part of the body. Here the wave drag will be very high and the shock wave, being so strong in this inboard position, would be detrimental to any rear propulsion system integration. The lower surface pressure distribution highlights the high pressures along the leading edge attachment line, as well as the rapid pressure recovery towards the trailing edge around the rear crank. There also appears to be a wave like region of high pressure inboard near the leading edge crank, which appears to be due to a local bubble-like separation that existed in the steady RANS starting solution, but dissipated over the 1 second of physical time in the DDES solution. This was enough to contaminate the time averaged surface pressure plot, and could have been corrected had more physical time been simulated. At the higher 8^o angle of attack, the curving flow that appears ahead of the rear crank at $\alpha = 6^o$, has now evolved into a strong, fully fledged tornado like vortex, together with a smaller weaker vortex further outboard. The flow is also seen to be fully separated from the leading edge from about 70% span. The formation of this vortex is seen to unsweep the shock wave ahead of it, and the flow in this vicinity is highly unsteady, with the shock rippling upstream and downstream by a distance of about 5% on the centerline chord.

By 10^o angle of attack the tornado vortex feature still exists but is considerably reduced in strength. It is strong enough, however, to cause a pronounced kink in the shock wave structure close to the leading edge crank. By now the stall front, where the leading edge is separated, has progressed inboard to around 60% span, and the stall cell associated with the tornado vortex, and the secondary feature further outboard, has grown in size, but there is still some attached flow ahead of it. The response of the shock wave is seen to be a forward movement towards the nose, being normal to the freestream over most of its extent. The lower surface pressure distribution does not significantly change with incidence. Finally, at the highest angle of attack investigated, $\alpha = 12^o$, the outboard flow is predicted to have completely broken down into deep stall, with only the flow on the inner 25% of the span, where the body is thickest, remaining attached. The upper surface shock wave is now predicted to have moved further upstream to be a normal shock wave spanning the inboard body from the leading edge crank. By this stage in a pitch-up, the notional propulsion system mounted on the rear upper surface would be ingesting highly separated airflow at the outer extent of its intake.

The results of this study indicate that the high speed transonic stall process is a highly complex mechanism for a blended wing body configuration – far more complex than is seen on more conventional swept and tapered wings currently employed on civil airliners. These complex flows, involving tip stalls, tornado vortex formations and their interaction with the upper surface transonic shock wave must be better understood, particularly from a propulsion integration perspective. The authors hope that this paper will provide the spur for the investment into high quality, industrial scale transonic wind tunnel tests to provide the insight needed, and the experimental data necessary for method validation.

VI. Conclusion

The results from this study demonstrate that:

- The Viscous Full Potential method, coupling the solution of the full potential equations with the integral boundary layer equations represents both an accurate and highly efficient method for the aerodynamic analysis of transonic aircraft flows in the conceptual design stage of their development. It is shown that such methods, properly implemented, can yield data of almost equivalent accuracy as Navier-Stokes based CFD methods but at 0.5% - 2% of the physical time. With such an approach, integrating similar appropriate fidelity methods for structural analysis, propulsion analysis etc., conceptual designers can significantly improve the overall design productivity.

- The flow physics of the stall mechanism associated with blend wing-body configurations is far more complex than that experienced on more conventional swept-tapered wings. The mechanism appears to involve an initial tip stall but also involves highly 3D vortical flows inboard on the upper surface of the wing which significantly distort the transonic shock wave. This represents a considerable problem for propulsion integration. With this in mind the community should invest in some high quality experimental campaigns to build much greater understanding of the problem, and generate experimental data for the validation of the design and analysis methods.

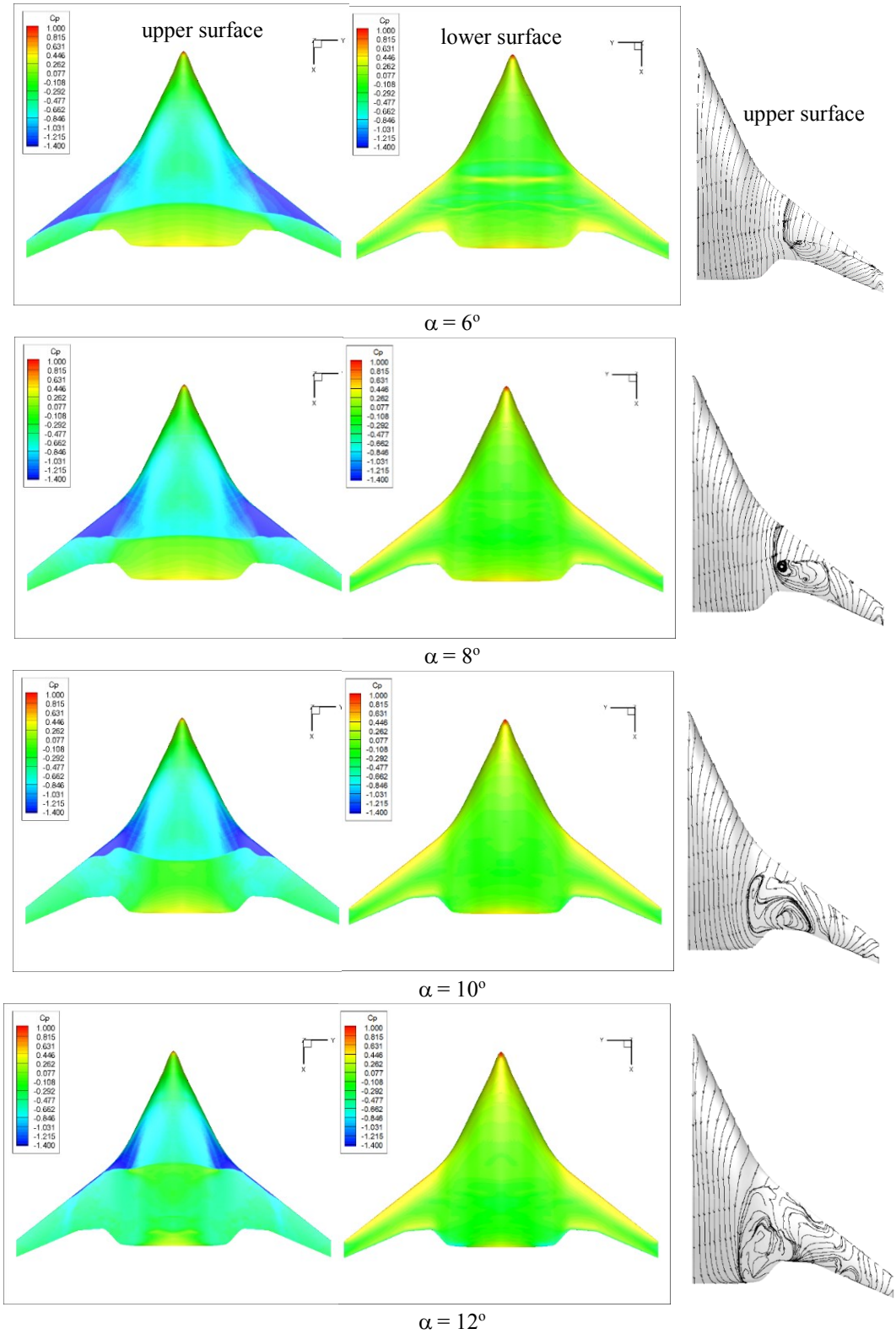

Fig. 10. The process of stall as resolved by the NS-DDES solver for M=0.85, Re_c = 7.4 x10^8. Instantaneous upper and lower surface pressure distributions and the corresponding upper surface skin friction lines are shown for the four angles of attack.

Acknowledgments

This work was funded by the British Government via the Aerospace Technology Institute / Innovate UK, together with Airbus UK Ltd., Rolls-Royce Ltd and GKN Ltd. The authors would also like to thank David Philpott and Kevin Hackett from ESDU, and Christina Nuzzo for their contributions to the project.

References

[1] Prince, S. A., Di Pasquale, D., Garry K. P. and Nuzzo, C., "A Rapid Aerodynamic Prediction Method for Unconventional Transonic Aircraft Configurations," ICAS Paper 2018-0138, 31st *International Congress of the Aeronautical Sciences* 2018. Belo Horizonte, Brazil, September 2018.

[2] Smith, P. D., "A calculation method for the turbulent boundary layer on an infinite yawed wing in compressible, adiabatic flow", *ARC CP* 1268. 1974.

[3] Full-potential (FP) method for three-dimensional wings and wing-body combinations – inviscid flow. Part I: Principles and results. ESDU 02013, June 2002 (with Amendment A, May 2006).

[4] Viscous full-potential (VFP) method for three-dimensional wings and wing-body combinations. Part 1: Validation of VFP results with experiment and comparisons with other methods. ESDU 13013.

[5] Von Karman, T. "Calculation of pressure distribution on airship hulls" NACA TM 574, 1930.

[6] De Jarnette, F. R., Ford, C. P. & Young, D. E. "A New Method for Calculating Surface Pressures on Bodies at an Angle of Attack in Supersonic Flow" AIAA Paper 79-1552. AIAA 12th Fluid & Plasma Dynamics Conference, Williamsburg, VA, July 1979. doi:10.2514/6.1979-1552

[7] Ashill, P. R. & Smith, P. D. "An integral method for calculating the effects on turbulent boundary layer development on sweep and taper", RAE Technical Report, TR83053. June 1983.

[8] Lawson, S. G, Greenwell, D. & Quinn, M. K. "Characterisation of Buffet on a Civil Aircraft Wing" AIAA Paper 2016-1309, AIAA 54th Aerospace Sciences Meeting, 4-8 Jan. 2016, San Diego, California, USA. doi:10.2514/6.2016-1309

[9] Barnola, R. L. "Interaction between Aerodynamics, Structure and Packaging in a Blended Wing Body Configuration Conceptual Design", Cranfield University MSc Thesis, 2012.

[10] Fielding, J. P. & Smith, S. "FLAVIIR, An Innovative University/Industry Research Program for Collaborative Research and Demonstration of UAV Technologies". ICAS Paper 2006-0278, 25th *International Congress of the Aeronautical Sciences* 2016. Hamburg, Germany, September 2006.

[11] Risch, T., Cosentino, G., Regan, D., Kisska, M. & Princen, N. "X-48B Flight-Test Progress Overview" AIAA Paper 2009-934, AIAA 47th Aerospace Sciences Meeting, 5-8 Jan. 2009, Orlando, Florida, USA. doi:10.2514/6.2009-934.